

Waves at walls, corners, heights: Looking for simplicity

J. A. C. Gallas^{1,2}, W. P. Schleich^{1,3}, J. A. Wheeler^{4,5}

¹ Max-Planck-Institut für Quantenoptik, D-85740 Garching, Germany

² Höchstleistungsrechenzentrum, Forschungszentrum Jülich, D-52425 Jülich, Germany

³ Abteilung für Quantenphysik, Universität Ulm, D-89069 Ulm, Germany
(Fax: +49-731/502-3086, E-mail: SCHLEICH@physik.uni-ulm.de)

⁴ Princeton University, Department of Physics, Princeton, NJ 08544, USA

⁵ Department of Physics, University of Texas at Austin, Austin, TX 78712, USA

Received: 25 October 1994 / Accepted: 7 December 1994

Abstract. We discuss the transition probability between energy eigenstates of two displaced “irrigation canal” potentials in its dependence on final state energy and wall steepness. We relate the probability caught underneath the Franck-Condon maximum to the missing probability in the corresponding problem of two displaced infinitely steep and infinitely high potential wells.

PACS: 03.65.Sq

The listener at a concert marvels at the smoothly flowing harmony that issues from instruments with sharp corners and mechanical keys. One magic key almost suffices to explain how these devices work: The wave analysis of Wentzel, Kramers and Brillouin (WKB) [1], when supplemented by three appropriate facilitators:

- (i) Attention to the demand for conservation of probability during every change of conditions, that is in space and time illustrated below by waves constrained between the two walls of an “irrigation canal” whose separation suddenly changes in time;
- (ii) Reflections arising from sudden changes in conditions of propagation;
- (iii) Corrections to the WKB-smooth propagation history arising from scattering at sharp corners.

In the present paper, we focus on the first point (i) and illustrate the demand for conservation of probability under sudden changes of the potential using two well-known and frequently used “Lehrbeispiele” of quantum mechanics: the potential well [2] and the irrigation canal [3] shown in Figs. 1 and 2, respectively.

The importance of this demand stands in sharp contrast to the apparent non-conservation of the transition probability

$$W_{m \leftarrow n}^{(\infty)} = \left| \int_{-\infty}^{\infty} dx u_m^{(\infty)}(x) v_n^{(\infty)}(x) \right|^2 \quad (1)$$

between the energy wave functions $u_m^{(\infty)} = u_m^{(\infty)}(x)$ and $v_n^{(\infty)} = v_n^{(\infty)}(x)$ of two slightly displaced potential wells of infinite height [4]. On the other hand, when we displace

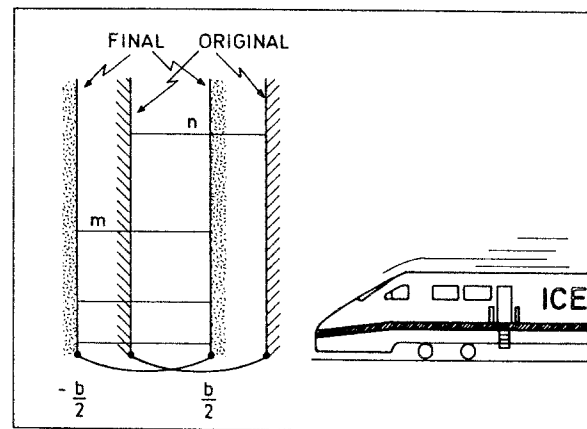


Fig. 1. Sudden displacement of an infinitely high and infinitely steep potential well by an amount x_0 . The abruptness of this process is illustrated here by the impact of an ICE train in full speed on the well. This sudden displacement induces sudden transitions between the n -th energy level of the original potential well of width b and the m -th level of the final well. To bring out the displacement most clearly in this figure we have rounded off the sharp corners and slightly curved the bottoms of these rectangular potentials

two irrigation canals as indicated in Fig. 3, the probability is conserved for every wall steepness κ (Fig. 4). Whereas in the present paper, we concentrate on the problem of the non-conservation of probability, the following paper [5] addresses in more detail points (ii) and (iii), that is, the phenomenon of WKB waves created at sharp corners of the potential which, in the present paper, makes its appearance (Fig. 5) as a modulation of the transition probability above the upper maximum.

In order to focus on the essential points, we have banished all lengthy calculations to Appendices. In Appendix A, we calculate the transition probabilities between the energy eigenstates of two shifted potential wells, whereas in Appendix B we derive the stationary wave functions, $u_m^{(\kappa)} = u_m^{(\kappa)}(x)$, of the irrigation-canal potential. We devote Appendix C to the evaluation of the integral over two displaced Airy functions [6] which arises in the evaluation of the transition probability between the energy eigenstates of

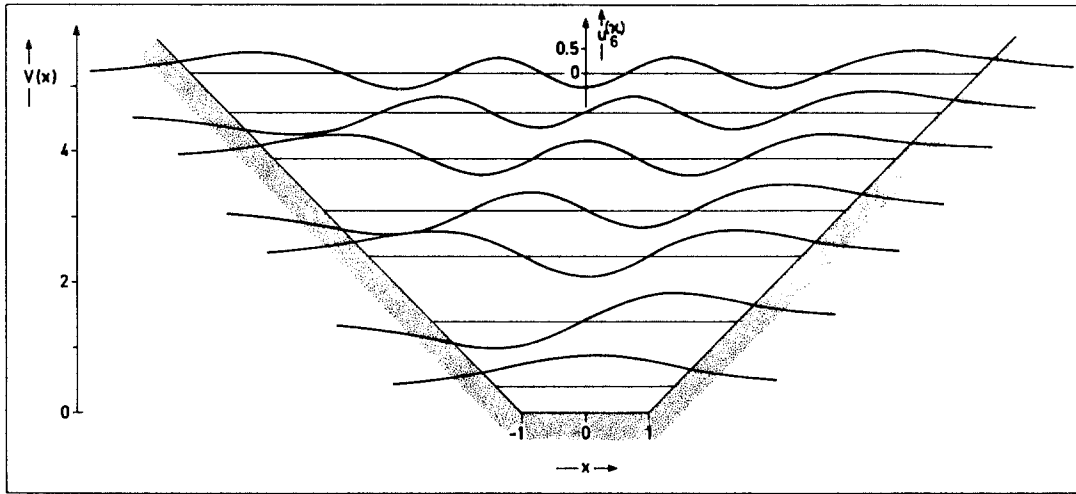


Fig. 2. The irrigation canal, $V = V(x)$ depicted here for a wall steepness, $\tau\kappa = 1$ and width $b = 2$, allows an analytical evaluation of the stationary wave functions $u_m^{(\kappa)} = u_m^{(\kappa)}(x)$. We only show the first seven states. The scale for the amplitudes of $u_m^{(\kappa)}$ is identical in all examples and is indicated for $m = 6$, only. The numerical value of the exact eigenenergies η_m — shown by *straight lines* in the potential — can be read off the scale for the potential energy on the left side of the figure

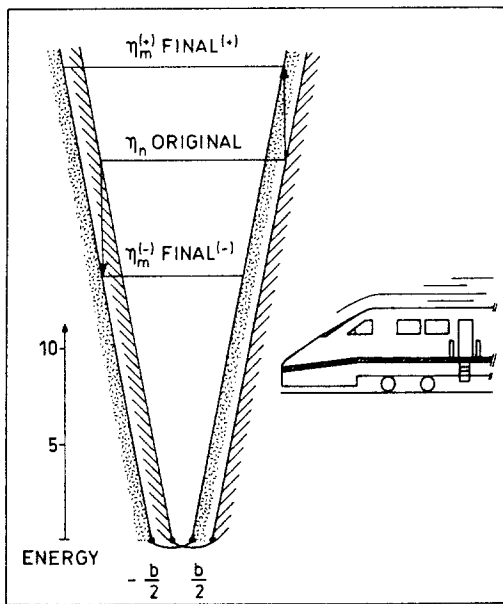


Fig. 3. A sudden displacement of the original irrigation canal keeping the wall steepness κ and the width of the canal constant populates the energy levels of the final canal. The reason and requirement for a high transition probability, that is, large occupation probability is identity of classical turning points for the motions in initial and final states as indicated by the *vertical lines*, $\eta_m^{(\pm)} = \eta_n \pm \kappa x_0$. Thus, the Franck-Condon principle favors transitions between energies η_n and $\eta_m^{(\pm)}$. As in Fig. 1, we have rounded off the sharp corners and have slightly curved the bottoms of these irrigation canals in order to bring out clearly the displacement of the potentials. (For this particular example, we have chosen $n = 10$, $b = 2$, $x_0 = 1$ and $\kappa = 5$)

two shifted irrigation canals performed in Appendix D. Appendix E offers physical insight into the dependence of the transition probabilities on the quantum state of the post-canal using the concept of area of overlap and interference in phase space [7].

1 The case of the missing probability

The old warning that the limit of a sum is not necessarily the sum of a limit is usually volant in physics only in such sophisticated contexts that it is often the practice to disregard it. However, there are familiar domains where this warning is well-taken. We here present the idealized problem of the displacement of a rectangular potential well that illustrates in sharp form this old point of calculus. The central issue manifests itself here in an apparent “non-conservation of probability”.

Take two displaced infinitely high and infinitely steep potential wells of width b as shown in Fig. 1; calculate, by following Appendix A, the corresponding Franck-Condon probabilities $W_{m \leftarrow n}^{(\infty)}$, of (1), for a transition from the n -th vibratory level of one potential to the m -th level of the other; recognize that, in the semi-classical limit [8], the occupation probabilities of the m -th level, summed over all m levels do not add to unity. Indeed, if the pre-canal and the post-canal overlap by x_0 , then

$$\sum_{m=0}^{\infty} W_{m \leftarrow n}^{(\infty)} = \sum_{m=0}^{\infty} \left| \int dx u_m^{(\infty)}(x) u_n^{(\infty)}(x) \right|^2 \cong 1 - x_0/b. \tag{2}$$

On the other hand, we recognize that the potential well of Fig. 1 grows out of the irrigation canal of Fig. 2 in the limit of infinite wall steepness κ . Consider therefore the transitions caused by the sudden displacement of two irrigation canals of identical steepness as shown in Fig. 3. Calculate, by following the Appendices B, C and D, the corresponding transition probability $W_{m \leftarrow n}^{(\kappa)}$ displayed in Fig. 4 as level occupation for several values of wall steepness κ . Note that for any (finite) value of the wall steepness the sum of these occupation probabilities over all m -levels does add to unity, that is,

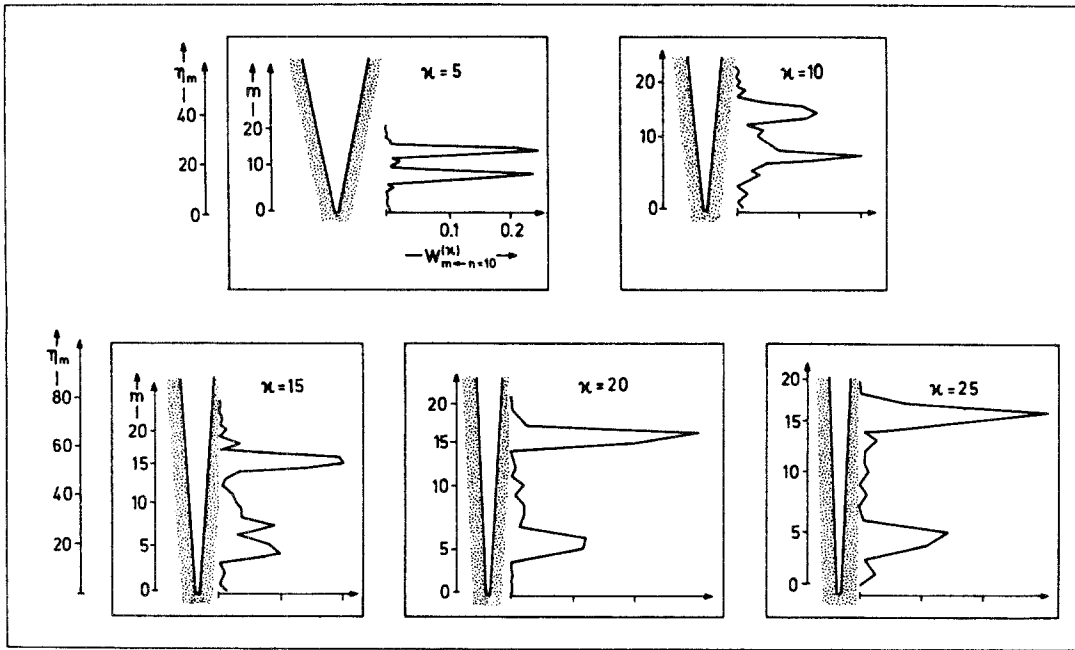


Fig. 4. Level occupation, that is, transition probability $W_{m \leftarrow n=10}$, in the post-canal after a sudden displacement of the pre-canal with initially only the state $n = 10$ being populated, for increasing steepness κ , but with identical width, $b = 2$, and displacement, $x_0 = 1$. The scale for $W_{m \leftarrow n=10}^{(\kappa)}$ on the *horizontal axis* is the same in all five examples. The location of the m -th energy level in the post-canal is indicated for each steepness κ by the nonlinear m -scale on the left-hand side of the potential. The energy scales η_m on the left-hand side of the figure apply to all figures in each row. For increasing κ , the (classical) Franck-Condon maxima, approximately located at $\eta_m^{(\pm)} = \eta_{n=10} \pm \kappa x_0$ climb higher in the canal, that is, shift towards higher energies while their separation, $2\kappa x_0$, grows. Moreover, the occupation probability at the Franck-Condon energies $\eta_m^{(\pm)}$ increases with increasing steepness

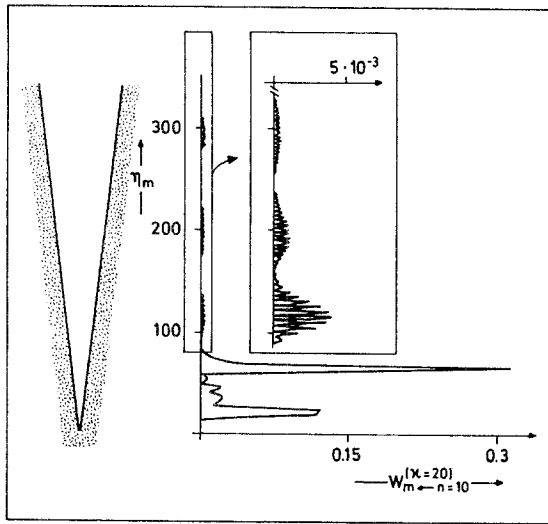


Fig. 5. The probability, $W_{m \leftarrow n=10}^{(\kappa)}$, for a transition to occur between the state $n = 10$ and the m -th state of excitation in two displaced irrigation canals is non-vanishing for energies η_m beyond the upper Franck-Condon energy. (Quasi-)periodical recurrences, that is, revivals of the probability, shown in detail in the insert, result from secondary waves created by scattering WKB waves off the sharp corners of the canal. (Here, we have chosen for the displacement $x_0 = 1$, $b = 2$ and a wall steepness $\kappa = 20$)

$$\sum_{m=0}^{\infty} W_{m \leftarrow n}^{(\kappa)} = \sum_{m=0}^{\infty} \left| \int dx u_m^{(\kappa)}(x) v_n^{(\kappa)}(x) \right|^2 = 1. \quad (3)$$

Nowhere clearer do we see that the limit of a sum is not necessarily the sum of limits, that is,

$$\lim_{\kappa \rightarrow \infty} \sum_{m=0}^{\infty} \left| \int dx u_m^{(\kappa)}(x) v_n^{(\kappa)}(x) \right|^2 \neq \sum_{m=0}^{\infty} \left| \int dx \lim_{\kappa \rightarrow \infty} u_m^{(\kappa)}(x) v_n^{(\kappa)}(x) \right|^2. \quad (4)$$

But where is the missing probability and what happened to it? These are the questions we address in the next section.

2 Case solved

In order to answer the questions raised in the previous section, we now return to the dependence (Fig. 4) of the transition probability $W_{m \leftarrow n}^{(\kappa)}$ between the energy eigenstates of two irrigation canals on the steepness κ of the walls. In this way, we relate the missing probability to the probability caught underneath the upper Franck-Condon maximum moving to higher and higher energies.

Let us start discussing first the qualitative behavior of $W_{m \leftarrow n}^{(\kappa)}$ in its dependence on the quantum number m of the post-canal, that is, the occupation probability of the m -th level of the final canal. For the sake of simplicity, we do not alter the steepness, κ , or the width, b , during the displacement process. Figure 3 displays the situation for the $n = 10$ -th energy eigenstate of an irrigation canal of width $b = 2$ and steepness $\kappa = 5$ displaced by an amount $x_0 = 1$.

According to the Franck-Condon principle [9], the requirement for high transition probability is identity of classical turning points for the oscillatory motion in the initial and final states, as indicated in Fig. 3 by the vertical lines.

The energies, $\eta_m^{(\pm)}$, of these final states are then given geometrically by

$$\eta_m^{(\pm)} = \eta_n \pm \kappa x_0. \quad (5)$$

Transition probabilities are not zero for states that fail the demand for identity of turning points. On the contrary, the probability $W_{m \leftarrow n}^{(\kappa)}$ oscillates as a function of m or η_m due to *interference in the phase space* [7], as discussed in Appendix E. We note that the numerical evaluation of the transition probabilities $W_{m \leftarrow n}^{(\kappa)}$ shown in Fig. 4 confirms this qualitative behavior predicted by semi-classical quantum mechanics.

We now turn to the discussion of the dependence of $W_{m \leftarrow n}^{(\kappa)}$ on the wall steepness.

In Fig. 4, we depict the irrigation canal for several values of wall-steepness κ . The energy scale, η_m , shown on the leftmost side of the figure is the same for the examples in each row. However, the location of the m -th energy level in these potentials, indicated on the left of each potential by the m -scale, is different for different κ . In particular, the ground state $m = 0$ is not located at the bottom of the canal. Moreover, the energy η_m , depends nonlinearly on the quantum number m , consequently the WKB energies (B12) follow a highly nonlinear m -scale. When we consider a fixed quantum number, say $m = 10$, the energy, $\eta_{m=10}$, of the corresponding level clearly increases for increasing wall steepness as shown in Fig. 4 and as indicated by (B12). In the final stage of $\kappa \rightarrow \infty$ however, the energy converges towards the κ -independent energy $\eta_{m=10}^{(\infty)}$ (A3) of the familiar rectangular potential well. We note, however, that for the κ -values depicted in Fig. 4 this regime has not been reached.

Horizontally, we depict the energy level occupation, $W_{m \leftarrow n=10}^{(\kappa)}$, for a sudden displacement of the irrigation canal by an amount $x_0 = 1$. For all examples, the scale on the horizontal axis is the same and the initial state is $n = 10$. We note two striking maxima of occupation probability at the Franck-Condon energies $\eta_m^{(\pm)}$ given by (4). The energy separation between the two maxima is approximately $2\kappa x_0$, in accordance with the classical Franck-Condon principle stated by (5).

For the depicted values of κ both Franck-Condon maxima $\eta_m^{(\pm)}$ move towards higher energies. This seems to be in contrast to (5), $\eta_m^{(-)} = \eta_{n=10} - \kappa x_0$, which might seem to suggest a shift towards lower energies. However, in this regime, the energy $\eta_{n=10}$ itself is an increasing function of the wall steepness κ , as discussed above and thus $\eta_{n=10}$ increases faster than the decrease of $\eta_m^{(-)}$ due to $-\kappa x_0$. In the final stage of the limit $\kappa \rightarrow \infty$, however, $\eta_{n=10}$ approaches the energy $\eta_{n=10}^{(\infty)}$ (A3) of the rectangular potential well and the decrease due to the $-\kappa x_0$ term can take over.

Hence, the two maxima in $W_{m \leftarrow n}^{(\kappa)}$ corresponding to transitions predicted by the classical Franck-Condon principle shift to higher and lower energies as κ increases. The area underneath each peak, however, does not decrease. For each value of κ the sum rule $\sum_m W_{m \leftarrow n}^{(\kappa)} = 1$ holds, that is, the probability is conserved. In the limit of $\kappa \rightarrow \infty$ both irrigation canals approach the case of infinitely high potential wells separated by an amount $x_0 < b$, where b is the width of the potentials. However, here the corresponding probability, $W_{m \leftarrow n}^{(\infty)}$, is not conserved, as shown in Sect. 1. The ‘‘missing’’ probability, x_0/b , represents the probability caught between the two infinitely steep wells, that is, the

upper Franck-Condon maximum, which has gone to heaven, illustrating in a most vivid way that the limit of a sum is not necessarily the sum of the limit.

3 Summary and outlook: Scattering from corners

In the present paper we have illustrated a problem associated with the most popular potential in quantum mechanics: Conditions where the potential well of infinite height seems to violate the demand of conservation of probability. This paradox stands out more clearly when we consider Franck-Condon transitions between two displaced potential wells of infinite height. The corresponding problem of transitions between two irrigation canals provides the clue about the case of the missing probability: For every value of wall steepness, the probability is conserved. However, as we increase the wall steepness, the upper Franck-Condon maximum climbs higher and higher in energy while the area underneath this peak stays essentially constant. We miss this peak, and hence the probability associated with it, when we first let the wall steepness go to infinity and then calculate the transition probability.

We conclude this article by presenting another striking effect which comes to light in the context of the irrigation canal. In Fig. 5, we show the occupation probability $W_{m \leftarrow n}^{(\kappa)}$ for a wall steepness of $\kappa = 20$. Apart from the two well-understood dominant Franck-Condon maxima and the oscillatory behavior in between, we observe a regular modulation of the transition probabilities above the upper Franck-Condon maximum. Underneath this modulation (amplified in the inset) lies a rapid oscillation in probability between neighboring quantum states. This structure in the transition probability beyond the Franck-Condon energy lies outside of the approach [7] that focuses on the area of overlap and interference in phase space and does not follow from semi-classical considerations of this type. It results from the interference of secondary WKB waves created by scattering the original WKB waves off the sharp corners of the irrigation canal. The treatment of sharp corners is the subject of the paper following this one [5].

Appendix A

Transition probabilities between two shifted potential wells

In this Appendix, we discuss the probability, $W_{m \leftarrow n}^{(\infty)}$, for a transition to occur from the n -th level of an infinitely high potential well of width b to the m -th level of an identical potential shifted by an amount x_0 , where $0 \leq x_0 < b$, as shown in Fig. 1. In particular, we focus on the problem of non-conservation of the probability, that is, we show that in the semi-classical limit, that is, for $m, n \gg 1$

$$\sum_{m=0}^{\infty} W_{m \leftarrow n}^{(\infty)} \cong 1 - x_0/b. \quad (A1)$$

The wave functions $u_m^{(\infty)}$ of an infinitely high potential well read [2]

$$u_m^{(\infty)} = (2/b)^{1/2} \cos[(\eta_m^{(\infty)})^{1/2} x + m\pi/2], \quad (A2)$$

where

$$\eta_m^{(\infty)} = [\pi(m+1)/b]^2 \quad (\text{A3})$$

is the energy of the m -th level.

The transition probability, $W_{m \leftarrow n}^{(\infty)}$, is given by

$$\begin{aligned} W_{m \leftarrow n}^{(\infty)} &= \left[\int_{-b/2+x_0}^{b/2} dx u_m^{(\infty)}(x) u_n^{(\infty)}(x-x_0) \right]^2 \\ &= (2/b)^2 [I_{m,n}^{(c,c)}]^2, \end{aligned} \quad (\text{A4})$$

where, for $0 \leq x_0 < b$, the quantity $I_{m,n}^{(c,c)}$ following from (D3) reads

$$\begin{aligned} I_{m,n}^{(c,c)} &= \mathcal{E}_-^{(\infty)} \cos\{[(\eta_m^{(\infty)})^{1/2} + (\eta_n^{(\infty)})^{1/2}] \frac{x_0}{2} + (m-n) \frac{\pi}{2}\} \\ &+ \mathcal{E}_+^{(\infty)} \cos\{[(\eta_m^{(\infty)})^{1/2} - (\eta_n^{(\infty)})^{1/2}] \frac{x_0}{2} + (m-n) \frac{\pi}{2}\}, \end{aligned} \quad (\text{A5})$$

where

$$\mathcal{E}_{\pm}^{(\infty)} = \frac{\sin\{[(\eta_m^{(\infty)})^{1/2} \pm (\eta_n^{(\infty)})^{1/2}](b-x_0)/2\}}{(\eta_m^{(\infty)})^{1/2} \pm (\eta_n^{(\infty)})^{1/2}}. \quad (\text{A6})$$

In the limit of large quantum numbers m and n , that is, in the semi-classical limit [8], the non-resonant contribution of $I_{m,n}^{(c,c)}$ is of the order of $(1/m \sim 1/n) \ll 1$, that is, small compared to the resonant term $\mathcal{E}_-^{(\infty)}$ in (A5), and we neglect it. This reduces (A4) to

$$W_{m \leftarrow n}^{(\infty)} \cong 4 \mathcal{A}_{m,n} \cos^2 \phi_{m,n}, \quad (\text{A7})$$

where

$$\mathcal{A}_{m,n} \equiv \frac{\sin^2[(m-n)\pi(b-x_0)/2b]}{\pi^2(m-n)^2}, \quad (\text{A8})$$

and

$$\phi_{m,n} = \frac{\pi}{2} [(m+n+2) \frac{x_0}{b} + m-n]. \quad (\text{A9})$$

In the last step, we have used (A3). From (A8), we immediately note that the main transition will occur for $m=n$.

We now test the conservation of probability. From (A7), we find

$$\begin{aligned} \sum_{m=0}^{\infty} W_{m \leftarrow n}^{(\infty)} &= 4 \sum_{m=0}^{\infty} \mathcal{A}_{m,n} \frac{1}{2} [1 + \cos(2\phi_{m,n})] \\ &\cong 4 \sum_{m=0}^{\infty} \mathcal{A}_{m,n} \frac{1}{2} \\ &\cong \frac{2}{\pi^2} \int_0^{\infty} dm \frac{\sin^2[(m-n)\pi(b-x_0)/2b]}{(m-n)^2}. \end{aligned}$$

In the third step, we have neglected the second contribution due to the rapid variation of $\cos(2\phi_{m,n})$. When we now introduce the variable $\lambda = (m-n) \frac{\pi}{2} (1 - \frac{x_0}{b})$ and extend the integral to minus infinity since $n \gg 1$, we arrive at

$$\sum_{m=0}^{\infty} W_{m \leftarrow n}^{(\infty)} \cong (1 - \frac{x_0}{b}) \frac{1}{\pi} \int_{-\infty}^{\infty} d\lambda \frac{\sin^2 \lambda}{\lambda^2} \quad (\text{A10})$$

which, when integrated [11], gives (A1). Thus, the probability is not conserved.

We can easily identify the ‘‘missing probability’’, x_0/b , when we recall that according to (A2), the average probability density of the m -th state is

$$\overline{(u_m^{(\infty)})^2} = \frac{2}{b} \overline{\cos^2[(\eta_m^{(\infty)})^{1/2} x + m\pi/2]} = \frac{1}{b}.$$

The missing probability, x_0/b , is thus the probability caught between the right wall of the pre-well located at $x = b/2 + x_0$, and the right wall of the post-well at $x = b/2$, that is, $(b/2 + x_0 - b/2) \cdot 1/b = x_0/b$.

We conclude this Appendix with a mathematical argument explaining the missing probability. When we calculate the transition probability $W_{m \leftarrow n}^{(\infty)}$, we expand the wave function, $v_n^{(\infty)}(x) = u_n^{(\infty)}(x-x_0)$, of the pre-well in terms of eigenfunctions, $u_m^{(\infty)}$, of the post-well. However, the wave functions $u_m^{(\infty)}$ are identically zero in the interval $b/2 \leq x \leq b/2 + x_0$, whereas the function $v_n^{(\infty)}$ is not. In this region, it is therefore impossible to represent $v_n^{(\infty)}$ by a combination of the $u_m^{(\infty)}$. As a result, this contribution of $v_n^{(\infty)}$ to the probability density, namely precisely x_0/b , is missing.

Appendix B

Wave functions and energy levels in an irrigation canal

In this Appendix, we derive the stationary wave functions, $u_m^{(\kappa)} = u_m^{(\kappa)}(x)$, of the irrigation-canal potential (Fig. 2). For the sake of simplicity, we suppress throughout this Appendix the superscript (κ) , indicating the dependence of the wave function on the wall steepness κ .

The stationary solutions u_m with eigenenergies η_m of the time-independent Schrödinger equation [4]

$$\frac{d^2}{dx^2} u_m(x) + [\eta_m - V(x)] u_m(x) = 0 \quad (\text{B1})$$

for the irrigation canal potential

$$V(x) = \begin{cases} -\kappa(x+b/2), & \text{for } x < -b/2 \\ 0, & \text{for } |x| \leq b/2 \\ \kappa(x-b/2), & \text{for } x > b/2 \end{cases}, \quad (\text{B2})$$

with steepness κ and width b , shown in Fig. 2, can be given in closed form. In the linear regime of V , that is, for $|x| > b/2$, the solution of (B1) satisfying the boundary condition, $u_m(x \rightarrow \pm\infty) = 0$, is the Airy function [6], Ai , of the appropriate argument [10]. For $|x| < b/2$, the solutions u_m consist of sine and cosine functions. Due to the symmetry of the potential V , u_m is either symmetric or antisymmetric around $x=0$ — depending on the quantum number m being even or odd. We are therefore led to the Ansatz

$$\frac{u_m(x)}{N_m} = \begin{cases} (-1)^m \text{Ai}[-\kappa^{-2/3} \eta_m - \kappa^{1/3}(x+b/2)] \\ \gamma_m \cos(\eta_m^{1/2} x + m\pi/2), \\ \text{Ai}[-\kappa^{-2/3} \eta_m + \kappa^{1/3}(x-b/2)] \end{cases}, \quad (\text{B3})$$

where the x domains of validity for each one of the three parts of $u_m(x)$ are the same respective ones appearing in the definition of $V(x)$ above. The coefficients N_m and γ_m and the energy eigenvalue η_m follow from the requirement of

(i) continuity of the wave function u_m at $x = \pm b/2$, that is,

$$\lim_{\varepsilon \rightarrow 0} u_m(\pm b/2 - \varepsilon) = \lim_{\varepsilon \rightarrow 0} u_m(\pm b/2 + \varepsilon), \quad (\text{B4})$$

(ii) continuity of the first derivative of u_m at $x = \pm b/2$, that is,

$$\lim_{\varepsilon \rightarrow 0} u'_m(\pm b/2 - \varepsilon) = \lim_{\varepsilon \rightarrow 0} u'_m(\pm b/2 + \varepsilon), \quad (\text{B5})$$

and

(iii) normalization of the wave function, that is,

$$\int_{-\infty}^{\infty} dx u_m^2(x) = 1. \quad (\text{B6})$$

Due to the symmetry already built into the *Ansatz*, (B3), the continuity conditions at $x = +b/2$ and $x = -b/2$ are identical.

From (B3) and (B4), we find immediately

$$\gamma_m = \frac{\text{Ai}(-\kappa^{-2/3}\eta_m)}{\cos(\eta_m^{1/2} b/2 + m\pi/2)}, \quad (\text{B7})$$

which, together with (B3) and (B5), yields the energy eigenvalue equation

$$\begin{aligned} & \cos(\eta_m^{1/2} b/2 + m\pi/2) \text{Ai}'(-\kappa^{-2/3}\eta_m) + \\ & \sin(\eta_m^{1/2} b/2 + m\pi/2) (\kappa^{-2/3}\eta_m)^{1/2} \text{Ai}(-\kappa^{-2/3}\eta_m) = 0. \end{aligned} \quad (\text{B8})$$

This highly transcendental equation has to be solved numerically. However, for large quantum numbers m , that is, in the semi-classical limit, or more precisely, for $z \equiv \kappa^{-2/3}\eta_m \gg 1$, the Airy function, Ai , and its derivative, Ai' , allow the asymptotic expansions [6]

$$\text{Ai}(-|z|) \cong \pi^{-1/2} |z|^{-1/4} \sin\left(\frac{2}{3}|z|^{3/2} + \pi/4\right) \quad (\text{B9})$$

and

$$\text{Ai}'(-|z|) \cong -\pi^{-1/2} |z|^{1/4} \cos\left(\frac{2}{3}|z|^{3/2} + \pi/4\right). \quad (\text{B10})$$

Equations (B9) and (B10) reduce (B8) to the cubic equation

$$(\eta_m^{1/2})^3 + 3\eta_m^{1/2} \frac{b\kappa}{4} + 2\left(\frac{-3\pi\kappa}{8}\right)\left(m + \frac{1}{2}\right) = 0, \quad (\text{B11})$$

which possesses only one real solution, namely [11],

$$\begin{aligned} & \eta_m^{(WKB)} \\ & = b\kappa \sinh^2\left\{\frac{1}{3} \text{arcsinh}[\kappa^{-1/2} 3\pi b^{-3/2} (m + 1/2)]\right\}. \end{aligned} \quad (\text{B12})$$

The approximate eigenvalue equation (B11) is identical to the one obtained from the semi-classical quantization condition [1]

$$\oint dx p_m(x) = 2\pi\left(m + \frac{1}{2}\right), \quad (\text{B13})$$

where

$$p_m(x) \equiv [\eta_m^{(WKB)} - V(x)]^{1/2} \quad (\text{B14})$$

with the potential $V(x)$ (B1).

It is well-known that the quantization condition (B12) provides an excellent approximation of the energies for large quantum numbers, whereas for low lying energy levels some disagreement might arise. Moreover, when we increase the steepness, κ , of the potential, the range of energies for which

(B12) is a good approximation shifts to higher quantum numbers, as is also indicated by the condition $\kappa^{-2/3}\eta_m \gg 1$ necessary for the applicability of the expansions (B9) and (B10). This behavior is closely related to the fact that in the case of an extremely steep irrigation wall ($\kappa \cong 20$) the lowest quantum states feel essentially an infinitely steep potential well with an eigenvalue spectrum [2]

$$\eta_m^{(\infty)} = (\pi/b)^2 (m + 1)^2. \quad (\text{B15})$$

This spectrum follows also from (B8) in the limit $\kappa^{-2/3}\eta_m \ll 1$. This condition is, of course, in contrast to the limit $\kappa^{-2/3}\eta_m \gg 1$ employed in the derivation of (B11), which for $\kappa \rightarrow \infty$ yields

$$\eta_m^{(WKB)} = (\pi/b)^2 (m + 1/2)^2. \quad (\text{B16})$$

The difference between (B15) and (B16) in the factor 1/2 is due to the fact, that for an infinitely high potential well the factor 1/2 in the Kramers quantization condition has to be replaced by unity [1].

We conclude this Appendix by deriving the normalization constant N_m . When we substitute (B3) and (B7) into (B6) we find

$$\begin{aligned} 1 &= N_m^2 \left\{ \int_{-\infty}^{-b/2} dx \text{Ai}^2[-\kappa^{-2/3}\eta_m - \kappa^{1/3}(x + b/2)] \right. \\ & \quad + \gamma_m^2 \int_{-b/2}^{b/2} dx \cos^2(\eta_m^{1/2}x + m\frac{\pi}{2}) \\ & \quad \left. + \int_{b/2}^{\infty} dx \text{Ai}^2[-\kappa^{-2/3}\eta_m + \kappa^{1/3}(x - b/2)] \right\} \\ &= N_m^2 \left\{ 2\kappa^{-1/3} \int_{-\kappa^{-2/3}\eta_m}^{\infty} d\lambda \text{Ai}^2(\lambda) \right. \\ & \quad \left. + \gamma_m^2 \frac{b}{2} \left[1 + \frac{\sin(\eta_m^{1/2}b + m\pi)}{\eta_m^{1/2}b} \right] \right\}. \end{aligned} \quad (\text{B17})$$

We evaluate the integral of the square of an Airy function with the help of (C18), that is,

$$\begin{aligned} & \int_{-\kappa^{-2/3}\eta_m}^{\infty} d\lambda \text{Ai}^2(\lambda) \\ &= [\text{Ai}'(-\kappa^{-2/3}\eta_m)]^2 + \kappa^{-2/3}\eta_m [\text{Ai}(-\kappa^{-2/3}\eta_m)]^2 \end{aligned}$$

and finally arrive at

$$N_m^{-2} = \frac{2[\text{Ai}'(-\kappa^{-2/3}\eta_m)]^2}{\kappa^{1/3}} + K [\text{Ai}(-\kappa^{-2/3}\eta_m)]^2, \quad (\text{B18})$$

where

$$K \equiv \frac{2\eta_m}{\kappa} + \frac{b}{2} \frac{\eta_m^{1/2}b + \sin(\eta_m^{1/2}b + m\pi)}{\eta_m^{1/2}b \cos^2(\eta_m^{1/2}b/2 + m\pi/2)}. \quad (\text{B19})$$

The exact wave functions, $u_m = u_m(x)$, for the irrigation canal of (B2) are thus determined by (B3), (B7), (B18), (B19) and the solution of the energy eigenvalue equation (B8).

Appendix C

Integration of the product of shifted Airy functions

In view of the discussion of the transition probabilities between two displaced irrigation canals, we evaluate in this Appendix the integral

$$A(\xi; y) = \int_{\xi}^{\infty} dx \text{Ai}(x)\text{Ai}(x+y). \quad (\text{C1})$$

The integral

$$A(\xi; y=0) = \int_{\xi}^{\infty} dx \text{Ai}^2(x) \quad (\text{C2})$$

governing the normalization of the wave function u_m , (B17), is thus a special case of A .

We evaluate A by deriving a differential equation of fourth order for the integrand

$$f(x) = \text{Ai}(x)\text{Ai}(x+y) \quad (\text{C3})$$

which enables us to express $f(x)$ in terms of its derivatives. This expression is then straightforward to integrate.

We start by differentiating (C3), that is,

$$f'(x) = \text{Ai}'(x)\text{Ai}(x+y) + \text{Ai}(x)\text{Ai}'(x+y), \quad (\text{C4})$$

and

$$f''(x) = \text{Ai}''(x)\text{Ai}(x+y) + 2\text{Ai}'(x)\text{Ai}'(x+y) + \text{Ai}(x)\text{Ai}''(x+y), \quad (\text{C5})$$

where prime denotes differentiation with respect to x . With the help of the differential equation for the Airy function [6]

$$\text{Ai}''(x) - x\text{Ai}(x) = 0, \quad (\text{C6})$$

we find

$$f''(x) = (y+2x)f + 2\text{Ai}'(x)\text{Ai}'(x+y), \quad (\text{C7})$$

where we have used again the definition (C3). One more differentiation

$$f''' = 2f + (y+2x)f' + 2\text{Ai}''(x)\text{Ai}'(x+y) + 2\text{Ai}'(x)\text{Ai}''(x+y) \quad (\text{C8})$$

together with (C6) yields

$$f''' = 2f + (y+2x)f' + 2x[\text{Ai}'(x)\text{Ai}(x+y) + \text{Ai}(x)\text{Ai}'(x+y)] + 2y\text{Ai}'(x)\text{Ai}(x+y), \quad (\text{C9})$$

and (C4) leads to

$$f'''(x) = 2f + (y+4x)f' + 2y\text{Ai}'(x)\text{Ai}(x+y). \quad (\text{C10})$$

The fourth derivative reads

$$f'''' = 6f' + (y+4x)f'' + 2y[\text{Ai}''(x)\text{Ai}(x+y) + \text{Ai}'(x)\text{Ai}'(x+y)] \quad (\text{C11})$$

or

$$f'''' = 6f' + (y+4x)f'' + 2yxf' + 2y\text{Ai}'(x)\text{Ai}'(x+y), \quad (\text{C12})$$

and with the help of (C7), we finally arrive at

$$f'''' = 6f' + (2y+4x)f'' - y^2f. \quad (\text{C13})$$

From (C13), we find

$$f(x) = \frac{1}{y^2} [6f' + (2y+4x)f'' - f''''],$$

which, when substituted into (C1), yields

$$A(\xi; y) = \frac{1}{y^2} [-6f(\xi) - 2yf'(\xi) - 4\xi f'(\xi) + 4f(\xi) + f''(\xi)], \quad (\text{C14})$$

where we have also used the fact that

$$f(x \rightarrow \infty) = f'(x \rightarrow \infty) = f''(x \rightarrow \infty) = 0.$$

With the help of (C10), (C14) reduces to

$$A(\xi; y) = \frac{1}{y^2} [-yf'(\xi) + 2y\text{Ai}'(\xi)\text{Ai}(\xi+y)] \quad (\text{C15})$$

and we arrive with (C4) at

$$A(\xi; y) \equiv \int_{\xi}^{\infty} dx \text{Ai}(x)\text{Ai}(x+y) = \frac{1}{y} [\text{Ai}'(\xi)\text{Ai}(\xi+y) - \text{Ai}(\xi)\text{Ai}'(\xi+y)]. \quad (\text{C16})$$

In the limit $y \rightarrow 0$ we find

$$A(\xi; y=0) = \lim_{y \rightarrow 0} \frac{1}{y} \{ \text{Ai}'(\xi)[\text{Ai}(\xi) + \text{Ai}'(\xi)y] - \text{Ai}(\xi)[\text{Ai}'(\xi) + \text{Ai}''(\xi)y] \} \quad (\text{C17})$$

and, therefore, using (C6),

$$A(\xi; y=0) = \int_{\xi}^{\infty} dx \text{Ai}^2(x) = [\text{Ai}'(\xi)]^2 - \xi[\text{Ai}(\xi)]^2, \quad (\text{C18})$$

a known result [12].

Appendix D

Overlap between the wave functions of two displaced irrigation canals

In this Appendix, we calculate the overlap

$$w_{m,n} = \int_{-\infty}^{\infty} dx u_m^{(\kappa)}(x)u_n^{(\kappa)}(x-x_0)$$

between the wave functions $u_m^{(\kappa)}$ and $u_n^{(\kappa)}$ for two shifted irrigation canals.

We can perform the integration over the real line most easily by decomposing the range of integration into the domains in which the wave functions u_m and $v_n \equiv u_n(x-x_0)$ have been written down in Appendix B. These intervals are

$$\int_{-\infty}^{\infty} dx = \int_{-\infty}^{-b/2} dx + \int_{-b/2}^{-b/2+x_0} dx + \int_{-b/2+x_0}^{b/2} dx + \int_{b/2}^{b/2+x_0} dx + \int_{b/2+x_0}^{\infty} dx.$$

Making use of (B3), we arrive at

$$\mathcal{H}_{m,n} = N_m N_n [(-1)^{m+n} I_{m,n}^{(-,-)} + (-1)^n \gamma_m I_{m,n}^{(c,-)} + \gamma_m \gamma_n I_{m,n}^{(c,c)} + \gamma_n I_{m,n}^{(+,c)} + I_{m,n}^{(+,+)}]. \quad (\text{D1})$$

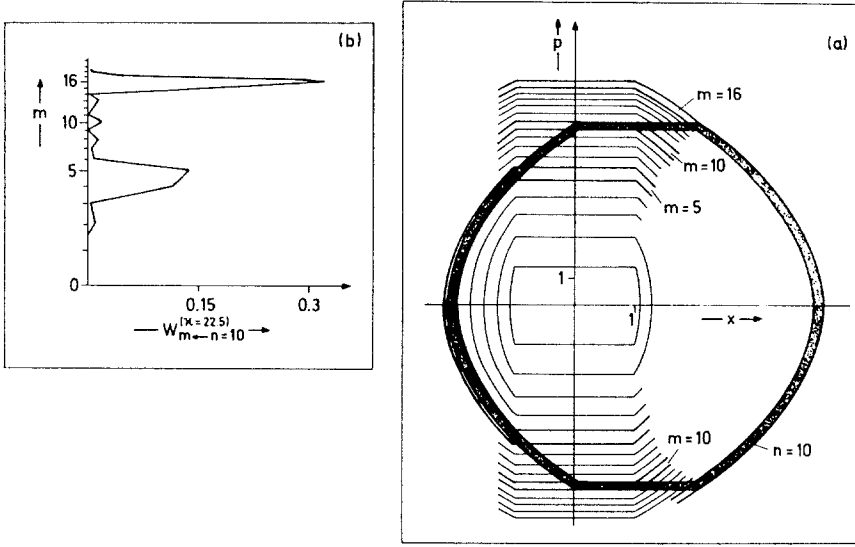


Fig. 6a,b. The Planck-Bohr-Sommerfeld bands, (E1) and (E3), corresponding to the energy eigenstates of the pre-canal with center at x_0 , steepness $\kappa = 22.5$, and width $b = 2$, take the shape of a race track as exemplified in (a) by the dark $n = 10$ band. According to the area-of-overlap concept, the probability, $W_{m \leftarrow n=10}^{(\kappa)}$, for a transition from the $n = 10$ state of the pre-canal to any m state of the post-canal with center at the origin and identical steepness κ and width b is governed by the overlap of the m -th race track whose edges are shown in (a) by solid lines, with the dark $n = 10$ band. The $m = 5$ and $m = 16$ bands have an unusually large area in common with $n = 10$ thus giving rise to a large transition probability. Bands corresponding to m values between these critical quantum numbers cross the n band in two interfering diamond-shaped areas creating an oscillatory transition probability. The area of cross-over of the other m bands with $n = 10$ is small, thus furnishing negligible values of $W_{m \leftarrow n=10}^{(\kappa)}$. These striking features of the transition probability brought to light by the area-of-overlap-plus-interference-in-phase-space concept are in complete accordance with the exact quantum-mechanical calculation of Appendix D, shown in (b). In order to relate horizontally the quantum number m to the m -th Planck band and its overlap with the $n = 10$ race track shown in (a), we use a highly nonlinear scale for the vertical m -axis

The integrals $I_{m,n}^{(-,-)}$, $I_{m,n}^{(c,c)}$, $I_{m,n}^{(+,+)}$, are defined by

$$\begin{aligned} I_{m,n}^{(-,-)} &= \int_{-\infty}^{-b/2} dx \text{Ai}\{-\kappa^{-2/3}[\eta_m + \kappa(x + b/2)]\} \\ &\quad \times \text{Ai}\{-\kappa^{-2/3}[\eta_n + \kappa(x - x_0 + b/2)]\} \\ &= \kappa^{-1/3} \int_{-\kappa^{-2/3}\eta_m}^{\infty} d\lambda \text{Ai}(\lambda) \\ &\quad \times \text{Ai}\{\lambda + \kappa^{-2/3}[\eta_m - (\eta_n - \kappa x_0)]\} \\ &= \mathcal{N}_- \{ \text{Ai}'(-\kappa^{-2/3}\eta_m) \text{Ai}[-\kappa^{-2/3}(\eta_n - \kappa x_0)] \\ &\quad - \text{Ai}'[-\kappa^{-2/3}(\eta_n - \kappa x_0)] \text{Ai}(-\kappa^{-2/3}\eta_m) \}, \quad (\text{D2}) \end{aligned}$$

where

$$\mathcal{N}_- = \frac{\kappa^{1/3}}{\eta_m - (\eta_n - \kappa x_0)},$$

$$\begin{aligned} I_{m,n}^{(c,c)} &= \int_{-b/2+x_0}^{b/2} dx \cos[\eta_m^{1/2}x + m\frac{\pi}{2}] \\ &\quad \times \cos[\eta_n^{1/2}(x - x_0) + n\frac{\pi}{2}] \\ &= \mathcal{E}_- \cos[\frac{1}{2}(\eta_m^{1/2} + \eta_n^{1/2})x_0 + (m - n)\frac{\pi}{2}] \\ &\quad + \mathcal{E}_+ \cos[\frac{1}{2}(\eta_m^{1/2} - \eta_n^{1/2})x_0 + (m - n)\frac{\pi}{2}], \quad (\text{D3}) \end{aligned}$$

where

$$\mathcal{E}_{\pm} = \frac{\sin\left[\left(\eta_m^{1/2} \pm \eta_n^{1/2}\right)(b - x_0)/2\right]}{\eta_m^{1/2} \pm \eta_n^{1/2}},$$

and

$$\begin{aligned} I_{m,n}^{(+,+)} &= \int_{b/2+x_0}^{\infty} dx \text{Ai}\{-\kappa^{-2/3}[\eta_m - \kappa(x - b/2)]\} \\ &\quad \times \text{Ai}\{-\kappa^{-2/3}[\eta_n - \kappa(x - x_0 - b/2)]\} \\ &= \kappa^{-1/3} \int_{-\kappa^{-2/3}\eta_n}^{\infty} d\lambda \text{Ai}(\lambda) \\ &\quad \times \text{Ai}\{\lambda - \kappa^{-2/3}[\eta_m - (\eta_n + \kappa x_0)]\} \\ &= \mathcal{N}_+ \{ \text{Ai}'(-\kappa^{-2/3}\eta_n) \text{Ai}[-\kappa^{-2/3}(\eta_m - \kappa x_0)] \\ &\quad - \text{Ai}'[-\kappa^{-2/3}(\eta_m - \kappa x_0)] \text{Ai}(-\kappa^{-2/3}\eta_n) \}, \quad (\text{D4}) \end{aligned}$$

where

$$\mathcal{N}_+ = \frac{-\kappa^{1/3}}{\eta_m - (\eta_n + \kappa x_0)}.$$

In obtaining (D2) and (D4) we have used (C16). Note that the denominators of the function \mathcal{N}_{\pm} vanish for the Franck-Condon energies $\eta_m^{(\pm)}$ (5). However at these energies also the numerators of (D2) and (D4) vanish, giving rise to maxima in $I_{m,n}^{(\pm,\pm)}$, the classical Franck-Condon maxima.

We have not been able to express the remaining integrals

$$\begin{aligned} I_{m,n}^{(c,-)} &\equiv \int_{-b/2}^{-b/2+x_0} dx \cos(\eta_m^{1/2}x + m\pi/2) \\ &\quad \times \text{Ai}\{-\kappa^{-2/3}[\eta_n + \kappa(x - x_0 + b/2)]\} \quad (\text{D5}) \end{aligned}$$

and

$$\begin{aligned} I_{m,n}^{(+,c)} &\equiv \int_{b/2}^{b/2+x_0} dx \text{Ai}\{-\kappa^{-2/3}[\eta_m - \kappa(x - b/2)]\} \\ &\quad \times \cos[\eta_n^{1/2}(x - x_0) + n\pi/2] \quad (\text{D6}) \end{aligned}$$

in closed analytical form and have therefore evaluated them numerically for various parameters of interest.

The overlap $w_{m,n}$ is thus given by (D1–D6), where the coefficients γ_j and N_j and the energies η_j for $j \equiv m, n$ follow from (B7), (B18) and (B8), respectively.

Appendix E

Transition probabilities between two shifted irrigation canals via interference in phase space

Deeper insight into the behavior of the transition probability $W_{m \leftarrow n}^{(\kappa)}$ between the n -th level of the irrigation canal of steepness κ and centered at x_0 to the m -th level of the identical canal centered at $x = 0$ springs from the concepts of area of overlap and of interference in phase space — the topic of the present Appendix.

This concept associates with the transition probability

$$W_{m \leftarrow n}^{(\kappa)} = \left| \int_{-\infty}^{\infty} dx u_m(x) v_n(x) \right|^2,$$

the *overlap in phase space* between the two quantum states u_m and v_n . But how to represent the two states? Let us consider the Planck-Bohr-Sommerfeld bands defined [7] in the $x - p$ phase space by their inner edge

$$\eta_m^{(\text{in})} = (p_m^{(\text{in})})^2 + V(x - x_0), \quad (\text{E1})$$

where $\eta_m^{(\text{in})}$ is determined from the quantization condition

$$\oint dx p_m^{(\text{in})}(x) = 2\pi m. \quad (\text{E2})$$

Their outer edge

$$\eta_m^{(\text{out})} = (p_m^{(\text{out})})^2 + V(x - x_0), \quad (\text{E3})$$

follows from the quantization condition

$$\oint dx p_m^{(\text{out})}(x) = 2\pi(m + 1). \quad (\text{E4})$$

Thus, each band takes up an area of 2π and the Kramers trajectory [7], governed by (B12) and (B13), runs in the middle of the band. The bands for the irrigation canal with center at $x = 0$ follow from (E1–E4) by replacing $V(x - x_0)$ by $V(x)$.

In Fig. 6a, we show the $n = 10$ -th band of the pre-canal by the solid race track. For this specific example, we have chosen the wall steepness $\kappa = 22.5$. The m -th track of the post-canal, whose edges are indicated in Fig. 6a by the solid lines, either does not overlap the $n = 10$ band (for $m < 4$ and $m > 16$), or gives rise to *one* unusually large tangential overlap (for $m = 4, 5$ or $m = 16$) or has *two* distinct diamond-shaped zones in common with the $n = 10$ band (for $5 < m < 16$). Hence, the transition probability $W_{m \leftarrow n=10}^{(\kappa)}$, governed by this area-of-overlap, is essentially zero for $m < 4$ and $m > 16$, but has maxima at $m = 5$ and $m = 16$. For intermediate quantum numbers, $5 < m < 16$,

the two diamond-shaped areas *interfere in phase space* [7], resulting in an oscillatory transition probability $W_{m \leftarrow n=10}^{(\kappa)}$ in complete agreement with the exact quantum-mechanical calculation shown in Fig. 6b.

Acknowledgements. One of us, J.A.C. Gallas, thanks Professor H.J. Hermann and Professor D. Wolf for their kind interest in his work and for many helpful discussions. We thank I. Bialynicki-Birula and S. Schaulfer for a critical reading of the manuscript.

References

1. For a review of the WKB method see, for example, M. V. Berry, K. E. Mount: *Rep. Prog. Phys.* **35**, 315 (1972)
J. A. Wheeler: *Studies in Mathematical Physics, Essays in Honour of Valentine Bargmann*, ed. by E. H. Lieb, A. S. Wightman (Princeton Univ. Press, Princeton 1976)
2. For the fundamental role of the rectangular potential well in quantum mechanics see, for example, D. Bohm: *Quantum Theory* (Prentice-Hall, Englewood Cliffs 1951)
3. For a discussion of the irrigation canal, see M. Casas, H. Krivine, J. Martorell: *Am. J. Phys.* **57**, 35 (1989)
4. Throughout this paper we use dimensionless variables $x = (2\mu\omega/\hbar)^{1/2}q$ and $p = (2\mu\hbar\omega)^{-1/2}\bar{p}$ where q and \bar{p} denote the dimensional coordinate and momentum of a particle of mass μ and ω is a characteristic frequency. The Schrödinger equation in these coordinates reads $i\dot{\Psi} = [p^2 + V(x)]\Psi$
5. J. Bestle, W. P. Schleich, J. A. Wheeler: *Appl. Phys. B* **60**, 289 (1995)
6. M. Abramowitz, I. E. Stegun (eds.): *Handbook of Mathematical Functions*, (National Bureau of Standards, Washington, DC 1964)
7. For a review of the concept of area-of-overlap and interference in phase space see, for example, J. P. Dowling, W. P. Schleich, J. A. Wheeler: *Ann. Phys. (Leipzig)* **48**, 423 (1991)
K. Vogel, W. P. Schleich: In *Fundamental Systems in Quantum Optics*, ed. by J. Dalibard, J. M. Raimond, J. Zinn-Justin (Elsevier, Amsterdam 1992)
8. For a nice discussion of the Bohr correspondence principle and the semi-classical limit we refer to M. Born: *Struktur der Materie in Einzeldarstellungen*, ed. by M. Born, J. Franck (Springer, Berlin 1925)
W. Pauli: In *Handbuch der Physik*, Vol. 24, ed. by H. Geiger, K. Scheel (Springer, Berlin 1933)
P. Debye: *Phys. Z.* **28**, 170 (1927)
9. See, for example, G. Herzberg: *Molecular Spectra and Molecular Structure I, Spectra of Diatomic Molecules* (von Nostrand, Princeton 1965) p. 169
E.U. Condon: *Am. J. Phys.* **15**, 365 (1947)
10. G. Breit: *Phys. Rev.* **32**, 273 (1928)
E. U. Condon, P. M. Morse: *Quantum Mechanics* (McGraw-Hill, New York 1929) p. 44
G. Süßmann: *Einführung in die Quantenmechanik* (Bibliogr. Institut Mannheim 1963) p.144
A. Das, A. C. Melissinos: *Quantum Mechanics, A Modern Introduction* (Gordon & Breach, New York 1986) p. 342
11. I. N. Bronstein, K. A. Semendjajew: *Taschenbuch der Mathematik* (Harri Deutsch, Zürich 1976)
12. A.P. Prudnikov, Yu.A. Brychkov, O.I. Marichev: *Integrals and Series*(Gordon & Breach, Moscow 1986) p. 33

This article was processed by the author using the L^AT_EX style file *pljour2* from Springer-Verlag.